Experiments in Fluids 26 (1999) 297–304 © Springer-Verlag 1999

Molecular Tagging Velocimetry (*MTV*) measurements in gas phase flows

B. Stier, M. M. Koochesfahani

Abstract Recent developments in Molecular Tagging Velocimetry (*MTV*) using the phosphorescence of biacetyl are described for gas-phase flows. With improvements in tagging, detection, and processing schemes, whole-field measurements of two components of the velocity vector are obtained simultaneously, typically at more than 300 points over a plane. Application of this measurement approach is demonstrated in mapping the velocity and vorticity fields of the intake flow into a "steady flow rig" model of an internal combustion engine.

1 Introduction

Molecular tagging approaches can offer attractive advantages for velocimetry in gas-phase flows compared to particle-based techniques (e.g. *PIV*), since issues such as the tracking of the flow by the seed particles are eliminated. In Molecular Tagging Velocimetry the flowing medium is premixed with molecules that can be turned into long-lifetime tracers upon excitation by photons of an appropriate wavelength. Typically a pulsed laser is used to "tag" small regions of interest. The tagged regions are imaged at two successive times within the lifetime of the tracer. The measured displacement vector provides the estimate of the velocity vector. This velocimetry approach yields whole-field, "instantaneous" maps of velocity vectors over a plane allowing the derivation of various kinematic quantities from the velocity field.

The majority of *MTV* developments in the past has occurred in liquid-phase flows. These applications have taken advantage of photochromic molecules (Popovich and Hummel 1967; Falco and Chu 1987; among others), caged fluorescent compounds (Lempert et al. 1995; Harris et al. 1996; among others), and specially engineered water-soluble phosphorescent supramolecules (e.g. Koochesfahani et al. 1993; Stier 1994; Hill and Klewicki 1996; Gendrich and Koochesfahani 1996; Gendrich et al. 1997). The review by Falco and Nocera (1993) discusses many of the efforts known at that time; a more recent summary of these developments is provided in Koochesfahani, et al. (1996).

For gas-phase applications, the use of excited-state oxygen fluorescence was pioneered by Miles et al. (1987, 1989, 1993) under the acronym *RELIEF*. This approach, which is currently the only one available for oxygen environments (e.g. air), requires three sources of photons of different wavelengths. The lifetime of the tracer (vibrationally excited O_2) is of the order of 100 μs, making it suitable for high-speed flows. The work described here relies on the phosphorescence of biacetyl, and requires one source of photons. However, its use is limited to oxygen-free environments due to the phosphorescence quenching by oxygen. The potential use of biacetyl for velocimetry was originally suggested by Hiller et al. (1984) in a demonstration experiment showing the displacement of a single tagged line by the flow, and later used by Lowry (1987) for velocimetry measurements at a single point. Liu et al. (1988) offered a method for making displacement measurements based on a grating, but did not perform actual flow field measurements. Multi-point velocity data were first reported in a two-stroke engine by Hilbert and Falco (1991) at 44 points acquired simultaneously.

The work presented here describes our recent developments in gas-phase *MTV* based on the use of biacetyl. These include improvements in tagging, detection, and processing which have lead to better accuracy and an increase in the number of measurement points by an order of magnitude. Application is demonstrated in the intake flow into a "steady flow rig" model of an internal combustion engine. Early descriptions of these developments have been given by Stier et al. (1995, 1996), along with a preliminary application to a forced jet flow (Stier and Koochesfahani 1997).

2 Properties of biacetyl

When using biacetyl as the molecular tracer for *MTV* applications, laser excitation is used to stimulate phosphorescence emission. The displacement of regions in the flow tagged in this manner is measured over a short time period within the phosphorescence lifetime, yielding the estimate of the velocity.

Received: *29 August 1997*/*Accepted*: *16 September 1998*

B. Stier, M. M. Koochesfahani
Department of Mechanical Engineering
Michigan State University
East Lansing, MI 48824, USA

Correspondence to: M. Koochesfahani

This work was supported by the MRSEC Program of the National Science Foundation, Award Number DMR-9400417. We would also like to thank Dr. Alfred Barney from the Chemistry Department at Michigan State University for his generous help and measuring the absorption and emission spectra in Figs. 1 and 2, and Mr. Colin MacKinnon for his help in revising the manuscript. Our *MTV* developments are a joint collaboration with Dr. Daniel Nocera, whose invaluable input is gratefully acknowledged

This section provides a brief description of the properties of biacetyl relevant to *MTV* measurements.

The properties of biacetyl ($CH_3COCOCH_3$, also called 2,3-Butanedione) have been studied extensively in the past (Okabe and Noyes 1957; Sidebottom et al. 1972; Badcock et al. 1972). It is non-toxic (actually a food additive), and its relatively high vapor pressure (40 Torr at room temperature) allows a molar seeding fraction of about 5%. The primary use of this tracer in fluid flow studies has been for flow visualization, as well as for quantitative density and concentration measurements using laser induced fluorescence diagnostics (e.g. Epstein 1977; McKenize et al. 1979; Paul et al. 1990; van Cruyningen et al. 1990). The absorption spectrum of biacetyl is shown in Fig. 1. The absorption data are shown over a wider wavelength range compared to previous flow studies, which have typically reported the absorption spectrum for wave-lengths above about $\lambda = 350$ nm. Note that the absorption increases below about $\lambda = 330$ nm and has a second peak at about 270 nm, consistent with the results reported by Jackson and Yarwood (1971) for a related compound, 2,3-Pentanedione. As will be shown later, the wavelength $\lambda = 308$ nm from the XeCl-filled excimer laser used in this study is suitable as a source of excitation.

The excitation of biacetyl leads to both fluorescence and phosphorescence emission, the latter of which is utilized for velocimetry. Since the phosphorescence is effectively quenched in the presence of oxygen, velocity measurements must be performed in oxygen-free flow; usually nitrogen is used as the flowing medium. The fluorescence lifetime is of the order of 10 ns, which is too short to be useful for the range of velocities found in most applications. The phosphorescence lifetime of biacetyl is reported to be as high as 1.5 ms (Sidebottom et al. 1972). As described by Hiller et al. (1984), the observed lifetime can be lower due to a variety of reasons. For example, lifetime decreases with increasing photon flux, primarily due to triplet–triplet annihilation. Also, unless all oxygen is completely purged from the flow system, a reduction in lifetime follows. Consistent with these observations, we have measured a lifetime of about 0.1 ms in this work using a 1 mJ beam from an excimer laser ($\lambda = 308$ nm).

In order to determine the optimum choice of laser wavelength, the phosphorescence emission spectrum is measured for excitation frequencies of $\lambda = 308$ nm (XeCl excimer), 351 nm (XeF excimer), 355 nm (tripled *YAG*), in addition to the two wavelengths for the peak absorption (270 nm, and 420 nm). Results shown in Fig. 2 indicate the expected trend that the wavelength with more absorption leads to more phosphorescence emission. Note that the results for $\lambda = 351$ nm and 355 nm essentially coincide, and only the result for $\lambda = 355$ nm is shown. The data suggest that $\lambda = 308$ nm is a more efficient source of excitation (from the total phosphorescence emission point of view) compared to $\lambda = 351$ nm previously used for concentration studies. These results lead us to the choice of a XeCl-filled excimer laser ($\lambda = 308$ nm) for our gas-phase *MTV* developments among the readily available laser wavelengths in the energy range of 100 mJ per pulse (see also the section on Experimental Setup).

3 Experimental setup

3.1 Flow facility

Our implementation of gas-phase *MTV* is demonstrated in a steady flow rig model of an internal combustion (*IC*) engine. The flow system illustrated in Fig. 3 operates in a blow-down mode using a high-pressure nitrogen reservoir (gas cylinder). Appropriate pressure regulators and valves are used to adjust the flow speed. Biacetyl is introduced by bubbling nitrogen through a liquid biacetyl bath in a seeding chamber. A heating tape is wrapped around the seeding chamber to counteract the temperature reduction in the nitrogen due to expansion from the high-pressure reservoir and evaporative cooling, which result in a reduction of the biacetyl vapor pressure. The resulting biacetyl-endowed nitrogen stream flows into the test section through flow management units.

The steady flow rig consists of a quartz cylinder of radius $R_0 = 41$ mm, placed axisymmetrically around the nozzle with a valve body placed axisymmetrically inside the jet nozzle. In this case the flow exiting through the valve opening, which simulates the intake flow into an *IC* engine geometry, is in the form of an annular jet. The steady flow rig configuration is commonly used in the *IC* engine research community to study the fundamentals of the intake flow (e.g. Bicen et al. 1985). In

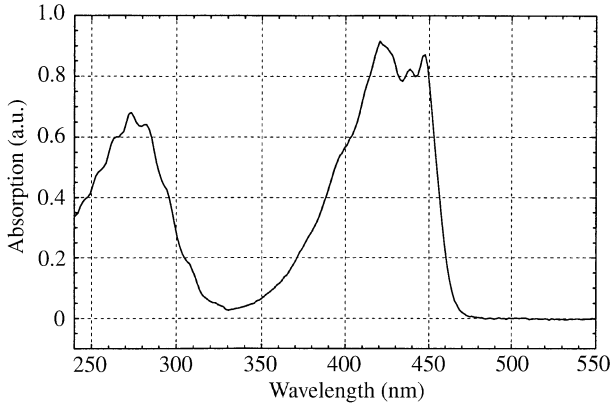

Fig. 1. Absorption spectrum for biacetyl

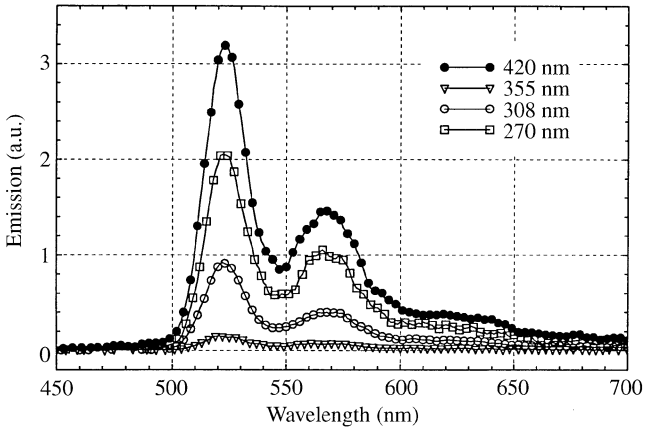

Fig. 2. Phosphorescence emission spectra for biacetyl for four different excitation wavelengths

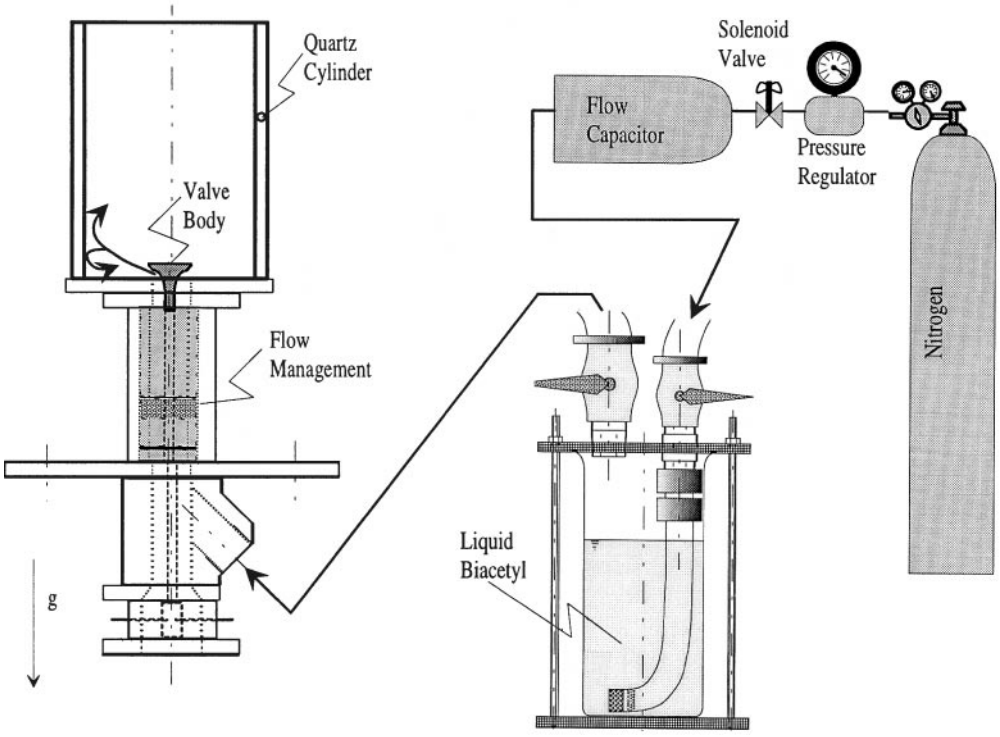

Fig. 3. Schematic of flow facility

this study, the valve opening (valve lift) is set at $\ell = 9$ mm and the maximum intake speed is about 10 m/s. The Reynolds number of the intake annular jet, based on the jet width and maximum speed at the jet centerline, is about 4200.

3.2
Tagging method and optical setup

The original work of Hiller et al. (1984) used tagging of the flow along a single line to demonstrate the viability of biacetyl's phosphorescence for velocimetry. Line tagging has also been the only method used to date in the works utilizing excited-state oxygen fluorescence (Miles et al. 1987, 1989, 1993). In this method, the velocity is determined from the displacement of the tagged lines in much the same manner as using hydrogen bubble lines generated by a wire (see for example Lu and Smith 1985). It is very important to recognize that line tagging allows the measurement of only one component of velocity, that normal to the tagged line. In addition, the estimate of this velocity component has an inherent error associated with it (see Hill and Klewicki 1996; Koochesfahani et al. 1996). Essentially the problem is connected with the ambiguity in the unique determination of the displacements of various portions of a (continuous) tagged line. This error can be minimized in some cases based on an *a priori* knowledge of the flow filed being measured.

In order to unambiguously measure two components of the velocity in a plane, the luminescence intensity field from a tagged region must have spatial gradients in two, preferably orthogonal, directions. For single-point velocimetry, this is easily achieved using a pair of crossing laser beams; a grid of intersecting laser lines allows mutli-point velocity measurements. Use of this tagging scheme was first suggested by D'Arco et al. (1982), and it was later improved upon and utilized by Falco and Chu (1987), who used photochromic molecules in liquid phase flows. In this work, we have used the simpler approach of Gendrich et al. (1997) for generating a grid of intersecting laser lines. The schematic in Fig. 4 illustrates the optical setup. The 20 ns, 150 mJ/pulse beam from an excimer laser(Lambda Physik LPX 220 iCC) is manipulated by cylindrical optics to increase its aspect ratio. The resulting beam is split by a 50 : 50 beamsplitter; each of the two resulting beams passes through a beam blocker to generate the laser grid pattern. The beam blocker is simply an aluminum plate with a series of thin slots. The spatial scaling of the entire grid pattern is controlled by appropriate lenses as needed. The inset in Fig. 4 shows an example of a region in a flow tagged in this manner. The energy in each beam in the grid is less than 1 mJ.

3.3
Detection and processing

The common element among most previous studies is that a single detector is used; the initial (or reference) tagging pattern is recorded once, usually at the beginning of the experiment, and then the "delayed" (with respect to the laser pulse) images are acquired. This approach works well as long as the initial tagging pattern remains spatially invariant throughout the experiment. Otherwise, any variations in the initial pattern (e.g. due to laser beam pointing instability, vibration of the optics, etc.) could be misinterpreted as flow velocity fluctuations. In the current work, the stability of the tagging pattern was confirmed by comparing a sequence of images tagged by different laser pulses, justifying the use of a single detector in these measurements. It is worth noting that in general a two-detector imaging system (see Gendrich

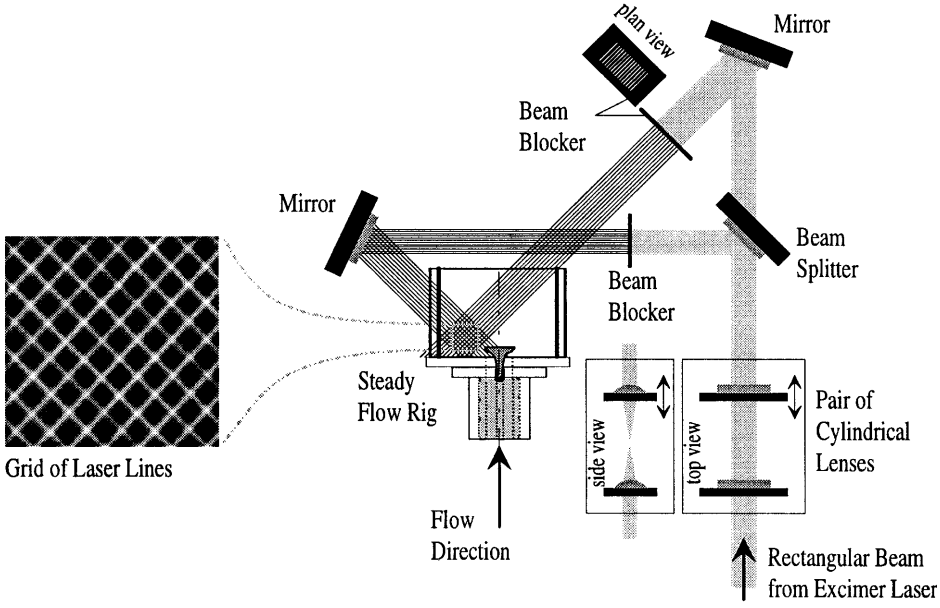

Fig. 4. Schematic of optical setup

et al. 1997 for details) allows for a more flexible system to accommodate cases where no assumption can be made *a priori* about the intensity field in a tagged region, e.g. due to non-uniform concentration of the tracer, or variations in the initial tagging pattern.

The experimental arrangement involves an image detector (Xybion ISG-350-GW3 gated image-intensified camera) which views the region of interest in the flow using a Nikon 50 mm *f*/1.2 lens along with appropriate close-up rings and extension tubes. The timing link between the laser and the image detector is established through a digital delay generator (Stanford Research Systems DG-535). A series of images of the initial tagging pattern is first recorded using successive laser pulses with the delay between the laser firing and image detection being negligibly small compared to the flow convection time. The average of these images forms the initial (reference) image. Then the later images (delayed image) of the tagged regions are recorded by the detector using a prescribed time delay, Δt, relative to the laser pulse. Images are digitized to 8 bits into a 512×512 pixel array by an image acquisition/processing system and transferred onto a high capacity (10 GB) disk array in real time.

The displacement of each grid intersection is determined using a direct digital spatial correlation technique. A small region surrounding a grid intersection in the reference image, referred to as the source window, is spatially correlated with a large roam window in the delayed image. The location of the peak of the correlation coefficient is identified as the displacement vector, which after division by Δt provides the estimate of the spatial average of the velocity within the source window. Sub-pixel accuracy is achieved using a polynomial fit to the region near the correlation peak. The details of this procedure and its performance are described in Gendrich and Koochesfahani (1996). A larger delay between the laser pulse and the acquisition of the delayed image will produce larger displacements and therefore a higher dynamic range in the velocity measurement. However, an increase in Δt leads to a degraded *S*/*N* in the delayed image (due to decay of phosphorescence intensity), and it can also produce large distortions due to the strain rate and vorticity fields, which can limit the effectiveness of the correlation procedure in estimating the displacement field. For the results described here the delay time was set to $\Delta t = 50$ μs corresponding to a maximum displacement of about 8 pixels ($\approx$ 500 μm). The gating period for the delayed image is typically set to be 10% of the delay period. Based on the results of Gendrich and Koochesfahani (1996) and the typical *S*/*N* of our delayed images, we expect that the displacements are determined to within $\pm$ 0.1 pixel with a 95% confidence limit (i.e. 95% of the displacement measurements are accurate to better than 0.1 pixel). This corresponds to a 95% confidence limit of 0.12 m/s for the instantaneous velocity measurements reported here.

It should be noted that the experimental setup for the measurements reported here was not arranged to resolve the smallest spatial scales of the flow. For example, the Kolmogorov length scale for the intake jet was estimated to be on the order of 10 μm and the Taylor microscale is about 400 μm. The size of the source window, optimally selected to be 2–3 times the width of the laser lines used for tagging based on the results of Gendrich and Koochesfahani (1996), is 25 pixels or 1500 μm in this case. This provides a conservative estimate for the upper bound of the size of the "measurement probe" in this particular setup. This size can be reduced by using thinner lines and correspondingly smaller source windows. This would require using appropriate optics for viewing smaller fields of view. It is also clear that flow information cannot be obtained over a time scale that is smaller than the time delay between tagging and interrogation.

4
Experimental results

Fig. 5a displays a 3 cm $\times$ 3 cm field of view in the nitrogen/biacetyl flow being investigated and regions tagged by a laser grid. This reference image is the average of 20 images

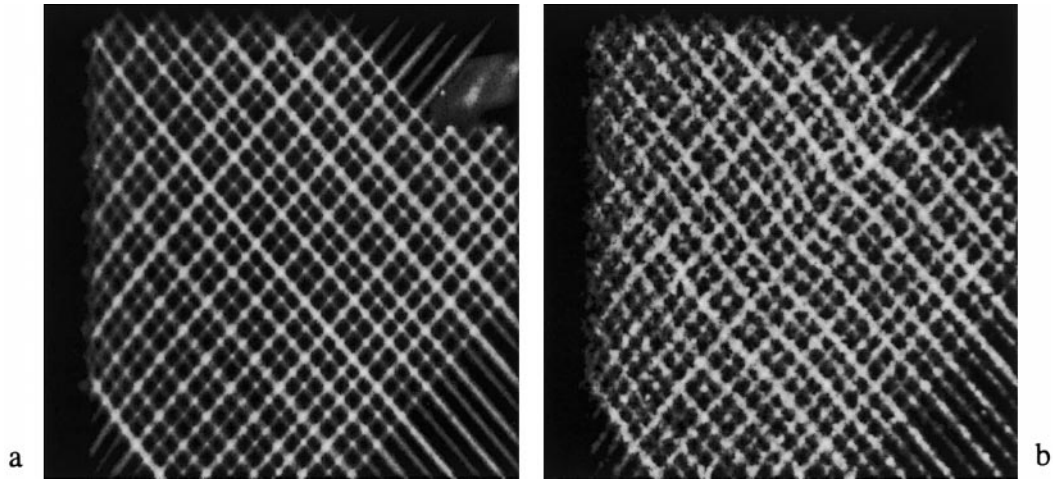

Fig. 5. Examples of **a** reference image and **b** instantaneous delayed (50 Os) image. The field of view is 3 cm × 3 cm

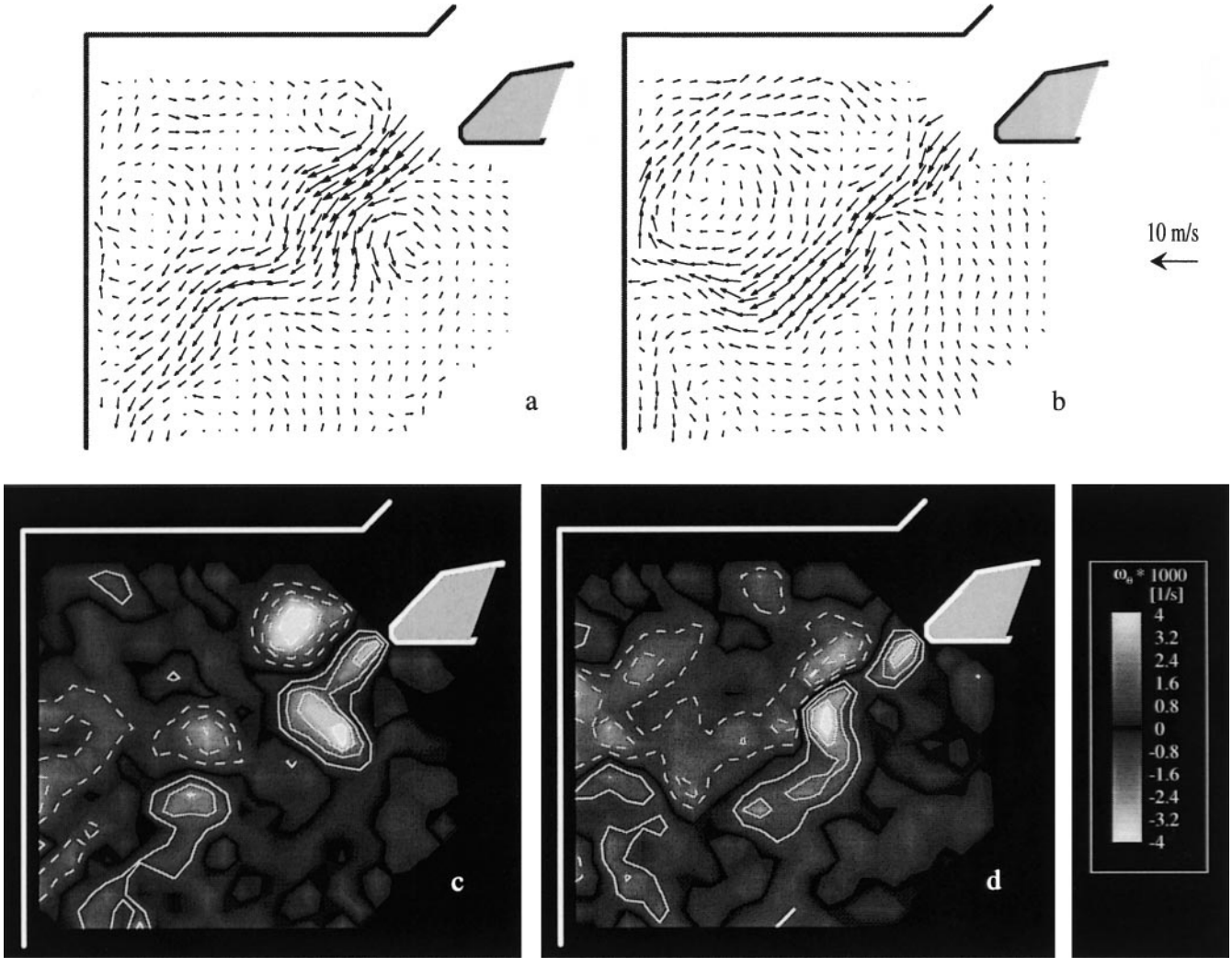

Fig. 6. Examples of **a,b** instantaneous velocity and **c,d** corresponding vorticity maps. Contour levels are ± 1,000, ± 2,000, ± 3,000, ... (s^{-1}). Dashed lines denote negative vorticity

acquired 200 ns after laser firing. Part of the valve body and the left wall of the cylinder are visible in the picture (note this image is flipped vertically compared to the schematic in Fig. 3). The maximum flow speed in the annular jet entering the cylinder is about 10 m/s. Fig. 5b is an example of the later image of the tagged regions after a 50 μs delay. The displacement and distortion of the tagged regions by the flow are apparent. Also apparent is the degradation of the S/N due to

the increase of the intensifier gain necessitated by the decrease of phosphorescence intensity.

Image pairs such as those in Fig. 5 are used to determine the instantaneous radial and axial velocity components, v_r and v_z, respectively. Two examples of the instantaneous velocity field are shown in Fig. 6a and b after being mapped onto a regular square grid of 1.2 mm spacing. The corresponding azimuthal vorticity field, $\omega_\theta = \partial v_z/\partial r - \partial v_r/\partial z$, is estimated using a second-order finite difference scheme, and is shown in Fig. 6c and d. The highly unsteady nature of this flow is apparent when comparing these two instantaneous flow maps. The intake annular jet has an undulating appearance with opposite sign large scale vortical structures on its two sides. The flow map in Fig. 6b indicates a large scale region of recirculation in the upper left corner of the engine cylinder. This feature, which will be more apparent in the average flow maps, is typical of an *IC* engine flow field.

The time-averaged velocity field was computed using 320 instantaneous realizations. The mean velocity field and the corresponding mean azimuthal vorticity field are illustrated in Fig. 7a and b. These mean flow maps clearly show the presence of the large scale recirculation zone in the upper left corner of the cylinder, a feature that does not always appear as coherent in the instantaneous velocity map (see Fig. 6a). The maximum level of the average vorticity in this recirculation region is rather low compared to the peak level of the average vorticity in the shear layers of the annular jet close to the valve body. Fig. 7a also highlights the sharp velocity gradients that occur on the two sides of the annular jet and the corresponding high levels of mean vorticity reaching peak levels as high as $4 \times 10^3\ s^{-1}$ (Fig. 7b). We note from the vorticity time series that the instantaneous vorticity level can reach peak levels more than 1.5 times higher than the peak of the average vorticity. In interpreting those vorticity levels, it is instructive to know that the uncertainty in the instantaneous vorticity measurements, in terms of the 95% confidence limit, is about $100\ s^{-1}$. This is determined based on the uncertainty in the velocity measurement and the grid spacing used for the finite difference calculation of the vorticity. It is also understood that the measured vorticity levels tend to give a lower bound to the actual values due to the spatial-averaging inherent in the measurements.

The maps of the rms of the velocity fluctuations in the axial (z) and radial (r) directions are depicted in Fig. 8a and b. It is interesting to note that the axial velocity fluctuation reaches its peak level on the lower edge of the annular jet shear layer; on the upper edge of the annular jet the fluctuations are much smaller (by about a factor of 2). We attribute this asymmetry to the presence of the large recirculation region next to the upper shear layer. In contrast to these observations, the map of the radial velocity fluctuation shows maximum values more in the middle of the annular jet and reduced levels towards the edges.

Whole-field maps such as these have not been previously available for this flow geometry; as a result, we are not able to compare our observations against previous data. Using point-wise *LDV* measurements, radial profiles of the mean and rms axial and radial velocity components have been reported by Bicen et al. (1985) for a steady flow rig of similar geometry (but slightly different parameters such as the valve opening and cylinder diameter). To compare with these profiles, we

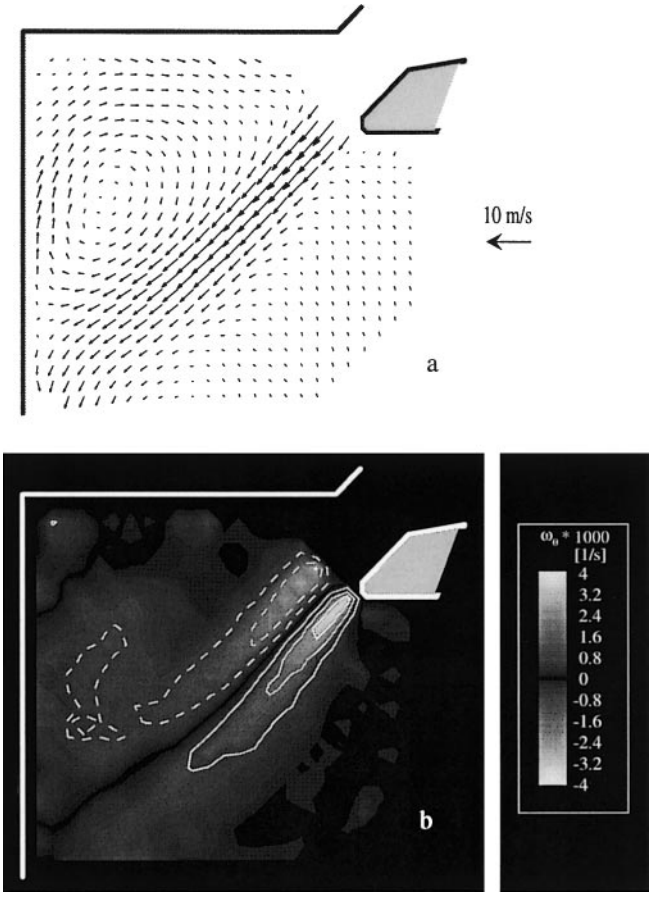

Fig. 7. Average **a** velocity and **b** corresponding vorticity map. Contour levels are $\pm$ 1,000, $\pm$ 2,000, ... (s^{-1}). Dashed lines denote negative vorticity

have extracted from our whole-field maps corresponding profiles at three different axial (z) locations; see Fig. 9. Also shown in this figure is a schematic of the positions of these three locations relative to the cylinder-valve geometry. Note that the peak values of axial (v_z) and radial (v_r) velocities are comparable owing to the mean angle of the annular jet being near 45°. Also note the change of sign in v_z as the cylinder wall is approached, a signature of the large recirculation zone in the upper left corner of the cylinder. The rms fluctuation levels are also comparable between the two components and reach very high values. The peak fluctuation level in the axial velocity is about 19% of the maximum annular jet centerline velocity of 10 m/s; or nearly 100% of the local mean axial velocity. These features are generally consistent with the previous *LDV* results of Bicen et al. (1985).

5 Conclusions

Recent developments in Molecular Tagging Velocimetry (*MTV*) in gas-phase are presented. This measurement technique can be thought of as the *molecular* counterpart of *PIV*, and because of its molecular nature, issues such as the tracking of the flow by the seed particles are eliminated. The work described here takes advantage of the long lifetime phosphorescence of biacetyl. Improvements in tagging, detection, and

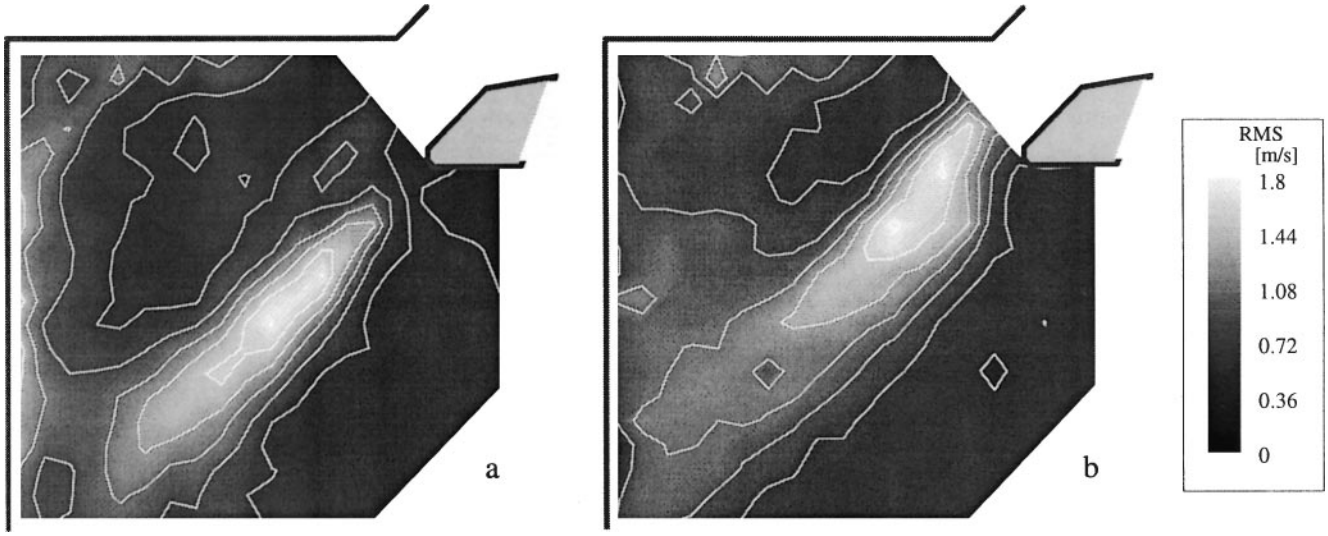

Fig. 8. **a** Axial, **b** radial RMS velocity fluctuation contour maps. Contour levles are 0.2, 0.4, 0.6, … (m/s)

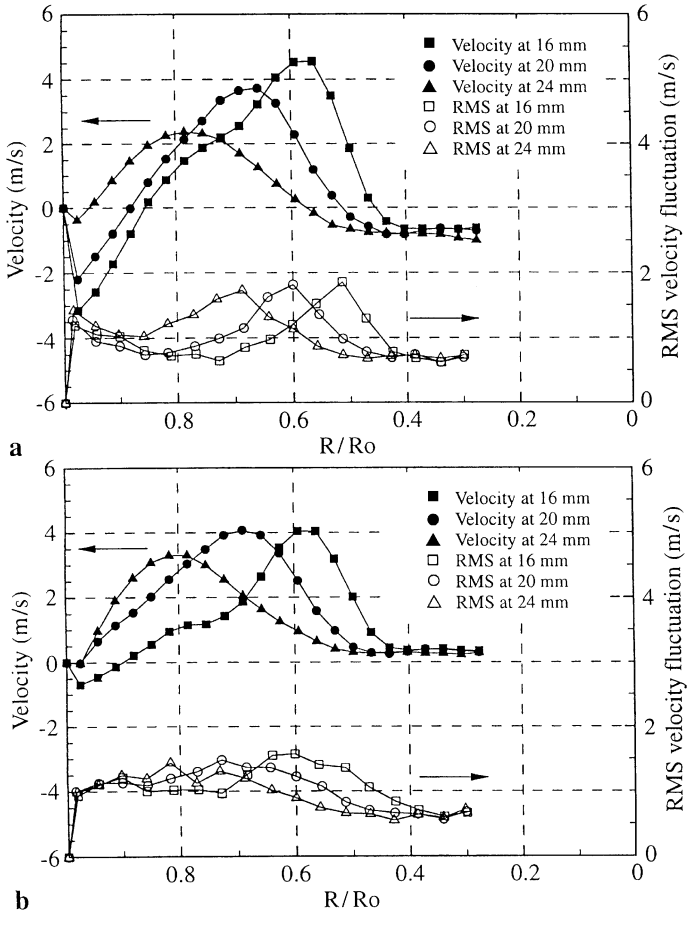

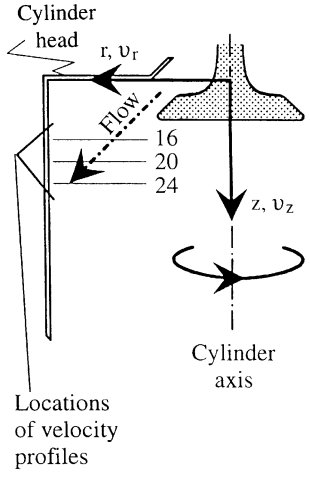

Fig. 9. Mean and RMS velocity profiles for the two velocity components **a** v_z and **b** v_r

processing schemes are described which have resulted in better accuracy and an increase in the density of measurement points. As a result, whole-field *MTV* measurements can now be carried out in gas phase flows in order to obtain the type of flow structure information previously available only through *PIV*. Application of this measurement approach is demonstrated in mapping the intake flow field of a "steady flow rig" model of an internal combustion engine. Typical radial profiles of the mean and rms velocities are extracted from these whole-field data and various features are highlighted. These features are

consistent with previous point-wise *LDV* measurements in a similar geometry.

While the focus of this study was the measurement of two components of the velocity vector, we note that the technique can be extended to provide three-component velocity data over a plane using stereo imaging with multiple cameras.

References

Badcock CC; Sidebottom HW; Calvert JG; Rabe BR; Damon EK (1972) A study of the triplet-triplet annihilation reaction in biacetyl vapor excited at 4365 Å and 25°. J Am chem Soc 94: 19–24

Bicen AF; Vafidis C; Whitelaw JH (1985) Steady and unsteady airflow through the intake valve of a reciprocating engine. J Fluids Engng 107: 413–420

Cruyningen I. van; Lozano A; Hanson RK (1990) Quantitative imaging of concentration by planar laser-induced fluorescence. Exp Fluids 10: 41–49

D'Arco A; Charmet JC; Cloitre M (1982) Nouvelle technique de marquage d'écoulement par utilisation de molécules photochromes. Rev Phys Appl 17: 89–93

Epstein AH (1977) Quantitative density visualization in a transonic compressor rotor. J Engng Power 99: 460–475

Falco RE; Chu CC (1987) Measurement of two-dimensional fluid dynamic qunatities using a photochromic grid tracing technique. Proc SPIE, Vol. 814, 706–710, San Diego

Falco RE; Nocera DG (1993) Quantitative multipoint measurements and visualization of dense solid–liquid flows using laser induced photochemical anemometry (LIPA). In Particulate two-phase flow. ed. M. C. Roco, Chapter 3, pp 59–126. Heinemann: Butterworth

Gendrich CP; Koochesfahani MM (1996) A spatial correlation technique for estimating velocity fields using molecular tagging velocimetry (MTV). Exp Fluids 22: 67–77

Gendrich CP; Koochesfahani MM; Nocera DG (1997) Molecular tagging velocimetry and other novel applications of a new phosphorescent supramolecule. Exp Fluids 23: 361–372

Harris SR; Lempert WR; Hersh L; Burcham CL; Saville DA; Miles RB; Gee K; Haughland RP (1996) Quantitative measurements of internal circulation in droplets using flow tagging velocimetry AIAA J 34: 449–454

Hilbert HS; Falco RE (1991) Measurements of flows during scavenging in a two-stroke engine. SAE Paper No. 910671

Hill RB; Klewicki JC (1996) Data reduction methods for flow tagging velocity measurements. Exp Fluids 20: 142–152

Hiller B; Booman RA; Hassa C; Hanson RK (1984) Velocity visualization in gas flows using laser-induced phosphorescence of biacetyl. Rev Sci Inst 55: 1964–1967

Jackson AW; Yarwood AJ (1972) Fluorescence and phosphorescence of 2,3-pentanedione. Can J Chem 50: 1331–1337

Koochesfahani MM; Gendrich CP; Nocera DG (1993) A new technique for studying the Lagrangian evolution of mixing interfaces in water flows. Bull Am Phys Soc 38: 2287

Koochesfahani MM; Cohn RK; Gendrich CP; Nocera DG (1996) Molecular tagging diagnostics for the study of kinematics and mixing in liquid phase flows. Proc Eighth Int Symp on Applications of Laser Techniques to Fluid Mechanics, pp 1.2.1–1.2.12, Lisbon, Portugal, 8–11 July

Lempert WR; Magee K; Ronney P; Gee KR; Haugland RP (1995) Flow tagging velocimetry in incompressible flow using PHoto-activated nonintrusive tracking of molecular motion (PHANTOMM). Exp Fluids 18: 249–257

Liu JB; Pan Q; Liu CS; Shi JR (1988) Principles of flow filed diagnostics by laser induced biacetyl phosphorescence. Exp Fluids 6: 505–513

Lowry HS (1987) Velocity measurements using the laser-induced phosphorescence of biacetyl. AIAA Paper 87–1529.

Lu LJ; Smith CR (1985) Image processing of hydrogen bubble visualization for determination of turbulence statistics and bursting characteristics. Exp Fluids 3: 349–356

McKenzie RL; Monson DJ; Exberger RJ (1979) Time-dependent local density measurements in unsteady flows. NASA Technical Memorandum 78555, Ames Research Center

Miles RB; Cohen C; Conners JJ; Howard PJ; Huang S; Markovitz EC; Russell G (1987) Velocity measurements by vibrational tagging and fluorescent probing of oxygen. Opt Lett 12: 861–863

Miles RB; Conners JJ; Markovitz EC; Howard PJ; Roth GJ (1989) Instantaneous profiles and turbulence statistics of supersonic free shear layer by Raman Excitation plus Laser-Induced Electronic Fluorescence (RELIEF) velocity tagging of oxygen. Exp Fluids 8: 17–24

Miles RB; Zhou D; Zhang B; Lempert WR; She ZS (1993) Fundamental turbulence measurements by RELIEF flow tagging. AIAA J 31: 447–452

Okabe H; Noyes WA (1957) The relative intensities of fluorescence and phosphorescence in biacetyl vapor. J Am Chem Soc 79: 801–806.

Paul PH; van Cruyningen I; Hanson RK; Kychakoff G (1990) High resolution digital flowfield imaging of jets. Exp Fluids 9: 241–251

Popovich AT; Hummel RL (1967) A new method for non-disturbing turbulent flow measurement very close to the wall. Chem Engng Soc 22: 21–25

Sidebottom HW; Badcock CC; Calvert JG; Rabe BR; Damon EK (1972) Lifetime studies of the biacetyl excited singlet and triplet states in the gas phase at 25°. J Am Chem Soc 94: 13–19

Stier B (1994) An investigation of fluid flow during induction stroke of a water analog model of an IC engine using an innovative optical velocimetry concept – LIPA, PhD Dissertation. Dept of Mech Eng, Michigan State University, East Lansing, Michigan

Stier B; Koochesfahani MM; Nocera DG; Schock HJ (1995) Molecular tagging velocimetry in gas phase flow. Bull Am Phys Soc 40: 1962

Stier B; Koochesfahani MM; Nocera DG; Schock HJ (1996) Velocity measurements in a steady flow model of an IC engine using Molecular Tagging Velocimetry. Bull Am Phys Soc 41: 1804

Stier B; Koochesfahani MM (1997) Molecular tagging velocimetry in gas phase and its application to jet flows. Proc ASME Fluids Engng Division Summer Meeting, Paper FEDSM97-3687, Vancouver, June 22–26